Eye-in-hand visual servoing of concentric tube robots

A. V. Kudryavtsev, A. Liadov, M. T. Chikhaoui, P. Rougeot, F. Spindler, K. Rabenorosoa, N. Andreff, and B. Tamadazte

***Abstract*—This paper deals with the development of vision-based controller for a continuum robot architecture. More precisely, the robotic structure that we seek to control is based on three concentric tube robot (CTR), an emerging technology to design accurate, miniature and flexible endoscopic robots. This technology has grown considerably in the recent years finding its applications in numerous surgical disciplines. In contrast to the rigid robotic structure, CTR kinematic arises many issues for an optimal control such as friction, torsion, shear, and non-linear constitutive behaviour. In fact, in order to ensure an efficient and a reliable control, in addition to computing an analytical complete kinematic model, it is also important to close the control loop. To do this, we developed an eye-in-hand visual servoing scheme using a millimetre camera embedded into the robot tip.**

Both the kinematic model and the visual servoing controller were successfully validated in simulation and using an experimental setup. The obtained results showed good performance of both the kinematic model and the visual servoing controller.

I. Introduction

Medical robotics has evolved more and more towards MIS (Minimally Invasive Surgery) and NOTES (Natural Orifice Transluminal Endoscopic Surgery) over the last ten years. Recent developments show particular interest in continuum robots (CR) and concentric tube robots (CTR), in particular [1]. Indeed, CTR paradigm provides a high level of dexterity in a confined space and enables to push the limits of miniaturization far away [2] compared to the cable or tendon driven CR [3], fluidic [4] or smart actuator based CR [5]. Several developments concern medical applications such as endonasal surgery, cardiac surgery, pulmonary surgery, etc. as reviewed in [1]. To achieve medical tasks, CTR can be teleoperated through a surgeon-robot interface or closed-loop controlled using exteroceptive sensors, usually medical images: MRI (Magnetic Resonnance Imaging) [6], CT (Computed Tomography) [7], US (Ultrasounds) [8], or more recently OCT (Optical Coherence Tomography) [9]) in an eye-to-hand configuration (when the camera views simultaneously both the robot and the scene). Some tasks require visual feedback to perform an automatic repetitive biopsy to follow-up cell evolution [10], achieve path following in image [11], and keep a tool in the field-of-view [8], [12] during interventions. In addition, the development of surgical robotic systems with two CR is increasing [13], [14]. In this case, the first CR brings a tool and the second one embeds the visualization system with a diameter smaller than 2 mm, e.g., miniaturized camera, OCT probe, or probe-based confocal laser endomicroscopy. An eye-in-hand configuration, i.e. a visual sensor mounted on the tip of the robot, is well suited to achieve the control of CR in endoscopic interventions. In contrast to a static camera, this configuration allows a more easy target recognition and inspection resulting from localization, the resolution of occlusion problem and limited depth-of-field, and spatial resolution [15]. As a result, with visual feedback, one can imagine the switch to fully automated tasks under the supervision of surgeons or physicians in order to improve safety, accuracy, and improve the intervention duration. To close the control loop, one can consider an image-based visual servoing (IBVS) scheme.

A model-free IBVS technique is proposed in [16] allowing to control the motion of a CTR limited to four degrees-of-freedom (DOF) (i.e. composed of 2 tubes). Authors proposed the use of an estimated Jacobian matrix which has to be updated for each cycle.

In this paper, we propose an IBVS for CTR in eye-in-hand configuration. The advantage of this approach is in the accurate calculation of the Jacobian and its ability to perform task redundancy control [17], [18]. The main contribution of this paper consists of the model-based eye-in-hand visual servoing of CTR which includes the derivation of the visual servoing method, the complete model of three tubes CTR and its implementation model in the Visual Servoing Platform (ViSP) [19], 6 DOF visual servoing simulation results and 3 DOF experimental results with adaptive control gain and tracking scenario for free-space positioning.

This paper is organized as follows. Section II introduces briefly the IBVS control scheme for the eye-in-hand configuration while section III details the three tubes CTR modeling and its implementation in ViSP library when Section IV presents the experimental validation of the proposed method.

II. Methods for Eye-in-Hand Visual Servoing

This section is devoted to the brief introduction of IBVS control for the eye-in-hand configuration and the derivation of the control law by considering the model-based approach.

A. Basics of Visual Servoing

The aim of all vision-based control schemes is to minimize an error $\mathbf{e}(t)$ which is typically defined by

$$\mathbf{e}(t) = \mathbf{s}(\mathbf{m}(t), \mathbf{a}) - \mathbf{s}^* \tag{1}$$

A. V. Kudryavtsev, A. Liadov, P. Rougeot, K. Rabenorosoa, N. Andreff, and B. Tamadazte are with FEMTO-ST Institute, Univ. Bourgogne Franche-Comté, CNRS, F-25000 Besanon, France rkanty@femto-st.fr

F. Spindler is with the Inria Rennes-Bretagne Atlantique, Campus universitaire de Beaulieu, Rennes 35042, France fabien.spindler@inria.fr

M. T. Chikhaoui is with the Laboratory for Continuum Robotics, Leibniz Universitaet Hannover, Appelstr. 11, 30167 Hanover, Germany.

where $\mathbf{m}(t)$ is a set of image measurements (e.g., the image coordinates of interest points, or the parameters of a set of image segments) and $\mathbf{a}$ is a set of parameters that represents potential additional knowledge about the system. These image measurements are used to compute a vector of k visual features, $\mathbf{s}(\mathbf{m}(t), \mathbf{a})$. The vector $\mathbf{s}^*$ contains the desired values of these features.

For now, we consider the case of controlling the motion of a camera with six degrees-of-freedom attached to the robot's end-effector. The nature of the visual features set $\mathbf{s}$ can be used as a classifying means. While the literature is broad on this subject and the community is constantly innovating, one can find the examples of usage of image key-points [20], lines [21], photometric visual servoing [22], [23], and more recently shearlet [24] and wavelet [25] for visual servoing approaches in case of medical robotics purposes.

Let the spatial velocity of the camera be denoted by $\mathbf{v}_c$=$[\mathbf{v}, \boldsymbol{\omega}]^\top$ with $\mathbf{v} = [v_x, v_y, v_z]^\top$ the instantaneous linear velocity of the origin of the camera frame and $\boldsymbol{\omega} = [\omega_x, \omega_y, \omega_z]^\top$ the instantaneous angular velocity of the camera frame. Finally, the relationship between $\mathbf{e}$ and $\mathbf{v}_c$ is given by

$$\dot{\mathbf{e}} = \mathbf{L_s}\mathbf{v}_c \tag{2}$$

where $\mathbf{L_s} \in \mathbb{R}^{6\times k}$ is called *interaction matrix* related to $\mathbf{s}$.

The most common approach to IBVS is to merely use equations (2) and (1) to construct the control law of the following form

$$\mathbf{v}_c = -\lambda\widehat{\mathbf{L}_\mathbf{s}^+}\big(\mathbf{s}(t) - \mathbf{s}^*\big) \tag{3}$$

where λ is a positive gain and $\widehat{\mathbf{L}_\mathbf{s}^+}$ is the Moore-Penrose pseudo-inverse of the interaction matrix $\mathbf{L_s}$.

B. Eye-In-Hand Configuration

Equation (3) corresponds to camera velocity that now needs to be transformed to the joint velocities. Hence, we use the following control law

$$\dot{\mathbf{q}} = -\lambda(\widehat{\mathbf{L}_\mathbf{s}}{}^c\mathbf{V}_e\,{}^e\mathbf{J}_e)^+\big(\mathbf{s}(t) - \mathbf{s}^*\big) \tag{4}$$

where ${}^e\mathbf{J}_e$ is robot Jacobian matrix expressed in the end-effector reference frame and ${}^c\mathbf{V}_e$ is the velocity twist matrix of the following form

$${}^c\mathbf{V}_e = \begin{bmatrix} {}^c\mathbf{R}_e & [{}^c\mathbf{t}_e]_\times\,{}^c\mathbf{R}_e \\ \mathbf{0}_{3\times3} & {}^c\mathbf{R}_e \end{bmatrix} \tag{5}$$

which is used to transform a velocity skew vector from the end-effector frame to the camera frame. The product $\widehat{\mathbf{L}_\mathbf{s}}{}^c\mathbf{V}_e\,{}^e\mathbf{J}_e$ is called task-Jacobian. In coming section, the derivation of the CTR kinematic and Jacobian, as well as all required equations, are provided.

Let us consider $\mathbf{s} = \mathbf{x} = (x, y)$ as the image-plane coordinates of a set of points. For a 3D point with coordinates $\mathbf{P} = (X, Y, Z)$ in the camera frame, which projects as a 2D point with coordinates $\mathbf{x} = (x, y)$, we obtain the projection equations

$$\begin{cases} x = \dfrac{X}{Z} = (u - c_u)/f\alpha \\ y = \dfrac{Y}{Z} = (v - c_v)/f\alpha \end{cases}$$

where (u, v) gives the coordinates of the image point expressed in pixel units. c_u and c_v are the coordinates of the principal point, f is the focal length, α is the ratio of the pixel dimensions. The interaction matrix $\mathbf{L_s}$ related to $\mathbf{x}$ is

$$\mathbf{L_s} = \begin{pmatrix} \frac{-1}{Z} & 0 & \frac{x}{Z} & xy & -(1+x^2) & y \\ 0 & \frac{-1}{Z} & \frac{y}{Z} & 1+y^2 & -xy & -x \end{pmatrix} \tag{6}$$

In the matrix $\mathbf{L_s}$, the value Z is the depth of the point relative to the camera frame. Therefore, any control scheme that uses this form of the interaction matrix must estimate or approximate the value of Z which can estimated at the desired position (i.e., Z^*).

III. CTR Modeling and Implementation in ViSP Library

A. CTR Modeling

In this section, the standard approach of modeling CTR under piecewise constant curvature assumption (PCCA) is presented in order to develop the geometric model, as well as the differential kinematics.

1) Standard approach: The standard approach, detailed in [26], assumes that for a CTR constituted of n overlapping tubes, one can decompose the final shape into m successive segments. Each of them is assimilated to an arc of a circle by considering the PCCA. The proposed continuum robot joint parameters are called configuration space of arc parameters (κ, ϕ, ℓ) where κ is the curvature, ϕ is the arc equilibrium plane, and ℓ is the arc length. The relationship $\theta = \kappa\ell$ defines the bending angle of the arc. Fig. 1 summarizes these parameters and presents the definition of the different axes.

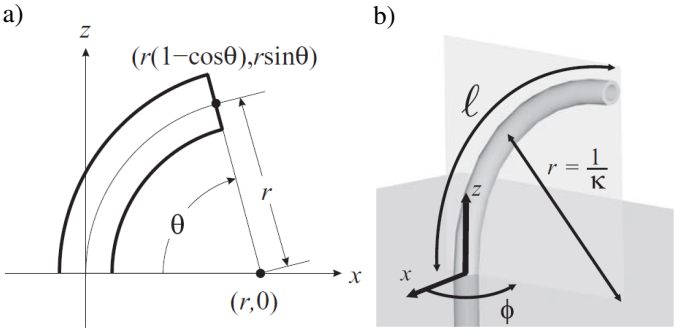

Fig. 1. a) The $x-z$ plane definition, when ϕ is zero. r designates the arc radius where $\kappa = 1/r$. b) Definition of the configuration space parameters, where the z- axis is defined as the arc principal axis [26].

Depending on the overlapping of the n tubes, the curvature of segment $j \in \{1...m\}$ is given by

$$\kappa_j = \sqrt{\kappa_{x_j}^2 + \kappa_{y_j}^2} \tag{7}$$

with

$$\begin{cases} \kappa_{x_j} = \frac{\sum_{i=1}^{n} E_i I_i \kappa_{i,j} c\theta_{i,j}}{\sum_{i=1}^{n} E_i I_i} \\ \kappa_{y_j} = \frac{\sum_{i=1}^{n} E_i I_i \kappa_{i,j} s\theta_{i,j}}{\sum_{i=1}^{n} E_i I_i} \end{cases} \tag{8}$$

where κ_x and κ_y are the decomposition of the main curvature along the $\mathbf{x}$ and $\mathbf{y}$ axes respectively, E_i is the elastic modulus, I_i is the cross sectional moment of inertia, $\kappa_{i,j}$ is the intrinsic

curvature of the i^{th} tube in the j^{th} segment, and $\theta_{i,j}$ denotes the i^{th} tube angle about the j^{th} segment frame $mathbf{z}$ axis, and c and s are cosine and sine functions respectively. The equilibrium plane angle is given by

$$\phi_j = \arctan(\kappa_{y_j}/\kappa_{x_j}) \tag{9}$$

A segment is defined whenever the number of the overlapping tubes is modified or the shape of a tube is different (straight or curved). The configuration for the case of three perfectly curved concentric tubes i (with $i \in \{1..n\}, n = 3$), the three segments j (with $j \in \{1..m\}, m = 3$) is displayed in Fig. 2.

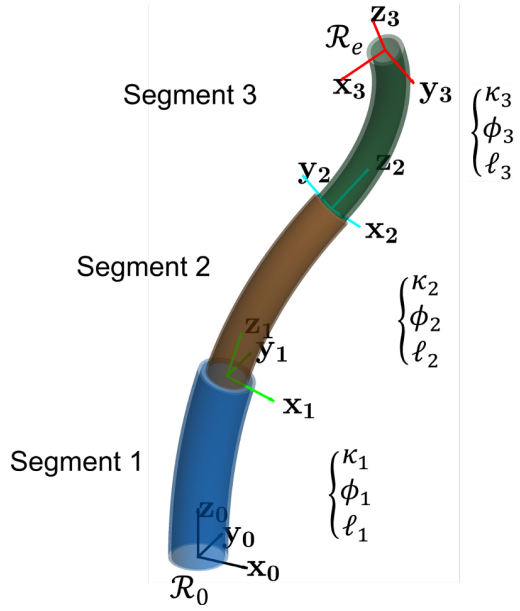

Fig. 2. Schematic description of segment distribution and arc parameters in the presence of three totally curved concentric tubes (outermost tube 1 in blue, middle tube 2 in brown, and innermost tube 3 in green). The general fixed frame is attached to the outermost tube basis, with the z-axis denoting the principal robot axis. A configuration frame is related to each segment end.

Previously mentioned parameters define the configuration space. Two other spaces were specified in [27] and can be summarized as follows: the *actuator space* $\{\mathbf{q}_i | i \in \{1..n\}\}$, the *configuration space* $\{\kappa_j, \phi_j, \ell_j | j \in \{1..m\}\}$, and the *task space* in $SE(3)$.

Two space transformations are thus defined

i. The *specific mapping* from the actuator space to the configuration space (actuator dynamics). This mapping totally depends on the actuation of the tubes.
ii. The *independent mapping* from the configuration space to the task space (forward kinematics). This mapping is generic as long as the CR architecture satisfies the assumption of constant curvature segments.

The transformation ${}^{j-1}\mathbf{T}_j$ from segment $j-1$ to segment j decomposes into a rotation of center $\mathbf{C}_j = [1/\kappa_j, 0, 0]^T$ about the $\mathbf{y}$ axis by θ_j and a rotation about the $\mathbf{z}$ axis by ϕ_j:

$${}^{j-1}\mathbf{T}_j = \begin{bmatrix} \mathbf{R}_z(\phi_j) & 0 \\ 0 & 1 \end{bmatrix} \begin{bmatrix} \mathbf{R}_y(\theta_j) & \mathbf{p}_j \\ 0 & 1 \end{bmatrix} \tag{10}$$

$${}^{j-1}\mathbf{T}_j = \begin{bmatrix} c\phi_j c\theta_j & -s\phi_j & c\phi_j s\theta_j & c\phi_j(1-c\theta_j)/\kappa_j \\ s\phi_j c\theta_j & c\phi_j & s\phi_j s\theta_j & s\phi_j(1-c\theta_j)/\kappa_j \\ -s\theta_j & 0 & c\theta_j & s\theta_j/\kappa_j \\ 0 & 0 & 0 & 1 \end{bmatrix} \tag{11}$$

where $\theta_j = \kappa_j \ell_j$ and $\mathbf{p}_j = [r_j(1-c\theta_j), 0, r_j s\theta_j]^\top$.

a) Independent Jacobian Matrix: The independent Jacobian computation relies substantially on the forward kinematics differentiation. The velocity of the j^{th} segment according to the segment $(j-1)$ is defined by

$${}^{j-1}\dot{\mathbf{X}}_j = \underbrace{\begin{bmatrix} c\Delta\phi_j(c(\kappa_j\ell_j)-1)/\kappa_j^2 & 0 & 0 \\ s\Delta\phi_j(c(\kappa_j\ell_j)-1)/\kappa_j^2 & 0 & 0 \\ -(s(\kappa_j\ell_j)-\kappa_j\ell_j)/\kappa_j^2 & 0 & 1 \\ -\ell_j s\Delta\phi_j & 0 & -\kappa_j s\Delta\phi_j \\ \ell_j c\Delta\phi_j & 0 & \kappa_j c\Delta\phi_j \\ 0 & 1 & 0 \end{bmatrix}}_{{}^{j-1}\mathbf{J}_{ind_j}} \begin{bmatrix} \dot{\kappa}_j \\ \Delta\dot{\phi}_j \\ \dot{\ell}_j \end{bmatrix} \tag{12}$$

where $\Delta\phi_j = \phi_j - \phi_{j-1}$ for $j \in \{2..m\}$ and $\Delta\phi_1 = \phi_1$.

Based on the adjoint transformation introduced by [28] and used in equation (5), the full independent kinematic Jacobian ${}^{e}\mathbf{J}_{ind_e}$ can be computed in the robot's end-effector frame. For a configuration with three totally curved CTR, we obtain ${}^{e}\mathbf{J}_{ind_e} \in \mathbb{R}^{6\times 9}$, as there are 3 segments as described in Fig. 2.

b) Specific Jacobian Matrix: The specific mapping depends essentially on the actuator structure and distribution along the CR. The derivatives of the curvature and equilibrium angle can be expressed with the same structure independently to the actuation. Differentiating (7) and (9) with respect to κ_x and κ_y yields

$$\begin{cases} \dot{\kappa}_j = \frac{1}{\sqrt{\kappa_{x_j}^2+\kappa_{y_j}^2}} \begin{bmatrix} \kappa_{x_j} & \kappa_{y_j} \end{bmatrix} \begin{bmatrix} \dot{\kappa}_{x_j} \\ \dot{\kappa}_{y_j} \end{bmatrix} \\ \dot{\phi}_j = \frac{1}{1+\kappa_{y_j}^2} \begin{bmatrix} -\kappa_{y_j} & \kappa_{x_j} \end{bmatrix} \begin{bmatrix} \dot{\kappa}_{x_j} \\ \dot{\kappa}_{y_j} \end{bmatrix} \end{cases} \tag{13}$$

where $\dot{\kappa}_{x_j}$ and $\dot{\kappa}_{y_j}$ are respectively the derivatives of κ_{x_j} and κ_{y_j} with respect to the actuators used in this case. The actuator space of CTR is defined by $\left\{\mathbf{q} = (\theta_i, .., \theta_n, \rho_i, .., \rho_n)^\top | i \in \{1..n\}\right\}$ where ρ_i and θ_i are the insertion length and angle of the i^{th} tube respectively.

Differentiating the j^{th} segment arc parameters leads to:

$$\begin{bmatrix} \dot{\kappa}_j \\ \dot{\phi}_j \end{bmatrix} = \underbrace{\begin{bmatrix} \frac{1}{\sqrt{\kappa_{x_j}^2+\kappa_{y_j}^2}} \begin{bmatrix} \kappa_{x_j} & \kappa_{y_j} \end{bmatrix} \\ \frac{1}{1+\kappa_{y_j}^2} \begin{bmatrix} -\kappa_{y_j} & \kappa_{x_j} \end{bmatrix} \end{bmatrix}}_{\mathbf{x}_j} \mathbf{A}_j \begin{bmatrix} \dot{\theta}_j \\ \vdots \\ \dot{\theta}_m \end{bmatrix} \tag{14}$$

with $\mathbf{A}_j = \frac{1}{\sum_{i=j}^{m} E_i I_i} \begin{bmatrix} -E_i I_i \kappa_{i,i} s\theta_i & \dots & -E_m I_m \kappa_{i,m} s\theta_m \\ E_i I_i \kappa_{i,i} c\theta_i & \dots & E_m I_m \kappa_{i,m} c\theta_m \end{bmatrix}$ for $i \in j..m$.

To summarize, after adding the segment length derivatives, the final arc parameter derivatives is

$$\begin{bmatrix} \dot{\kappa}_1 \\ \dot{\phi}_1 \\ \dot{\kappa}_2 \\ \dot{\phi}_2 \\ \dot{\kappa}_3 \\ \dot{\phi}_3 \\ \dot{\ell}_1 \\ \dot{\ell}_2 \\ \dot{\ell}_3 \end{bmatrix} = \underbrace{\begin{bmatrix} \mathbf{X}_1 & & & \mathbf{0}_{2\times3} \\ \mathbf{0}_{2\times1} & \mathbf{X}_2 & & \mathbf{0}_{2\times3} \\ \mathbf{0}_{2\times2} & & \mathbf{X}_3 & \mathbf{0}_{2\times3} \\ 0 & 0 & 0 & 1 & 0 & 0 \\ 0 & 0 & 0 & -1 & 1 & 0 \\ 0 & 0 & 0 & 0 & -1 & 1 \end{bmatrix}}_{\mathbf{J}_{spec}} \underbrace{\begin{bmatrix} \dot{\theta}_1 \\ \dot{\theta}_2 \\ \dot{\theta}_3 \\ \dot{\rho}_1 \\ \dot{\rho}_2 \\ \dot{\rho}_3 \end{bmatrix}}_{\dot{\mathbf{q}}} \quad (15)$$

with $\mathbf{J}_{spec} \in \mathbb{R}^{9\times6}$ is the specific Jacobian.

Finally, the full Jacobian matrix ${}^e\mathbf{J}_e$, utilized in equation (4), is calculated such that

$${}^e\mathbf{J}_e = {}^e\mathbf{J}_{ind_e}\mathbf{J}_{spec} \quad (16)$$

B. Implementation of CTR Model in ViSP

ViSP is a modular C++ multi-platform library that allows fast development of visual servoing applications. It was introduced since more than ten years [19] and the latest stable release can be downloaded `here`. The previously presented CTR models (15) and (11) are implemented in ViSP by following the library structure. Two classes were created based on *vpRobotTemplate*: *vpRobotCTR* and *vpSimulatorRobotCTR*. The contents of these classes is similar, both include the robot parameters and forward kinematics equations. However, the class *vpRobotCTR* also includes the code needed for the interaction with the real robot through UDP interface.

In order to obtain first validation of the model, the tests were performed with the simulator class. The robot needed to perform a simple task of achieving the desired position from different starting points. The simulation target contains four features, the minimal configuration needed to find the transformation between two images (similar to homography estimation [31]). The results of one simulation of 6 DOF robot control are displayed in Fig. 3. The error of positioning task is calculated as a sum of squared differences between point positions in image frame. It is important to note that the task is considered stopped when the error reaches the value of 10^{-5} m^2.

IV. Experimental Results

A. Experimental Setup

For the experimental validation, the prototype presented in Fig. 4 is used. The robot is controlled with the computer 1 (a 2.33 GHz Xeon Intel CPU). The computer 2 (an Intel Core TM with a 3.4 GHz processor) is exclusively dedicated to visual servoing tasks: image grabbing and processing, and computation of joint velocities. The latter is then sent to the first computer asynchronously using an UDP protocol. As mentioned previously, the system is mounted in an eye-in-hand configuration. This means that a camera (a MISUMI camera[1]) is placed on the robot tip (the camera weight is negligible and has no effect on the robot behavior). It produces images with resolution of 640 × 480 pixels with a frame-rate of 20 images per second. The CTR geometric features of the three tubes used to fabricate our CTR prototype are summarized in Table I.

[1]http://fr.misumi-ec.com/

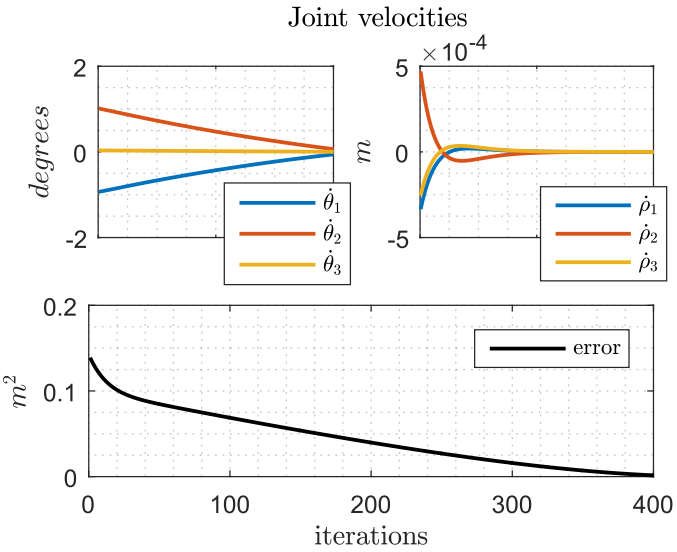

Fig. 3. 3D positioning of CTR: a) initial image and final image, b) evolution of RSM error.

TABLE I
Design parameters of the CTR prototype.

Tube i	Tube 1	Tube 2	Tube 3
Curvature κ_i (m^{-1})	4.91	7.2	9.76
Length L_i (mm)	120	155	200
Outer diameter (mm)	3.112	2.032	1.32
Wall thickness (mm)	0.222	0.279	0.180
Transmission length (mm)	0	200±50	400±50

Three types of tests were realized to study the performance of the proposed control scheme: automatic CRT positioning, the same with adaptive gain, and moving desired position. All of them are described below.

B. Automatic CRT Positioning

1) 3 DOF Positioning: The first step allowing the validation of the discussed approach consisted in automatic positioning of the CRT. The robot needed to perform a task of achieving the desired position from an arbitrary starting point. The target object is defined by four points (Fig. 5) that are then tracked during the operation. The model of the presented robot is now integrated in ViSP library and the main part of the code for the proposed visual servoing task is displayed in Listing 1. The results are shown in Fig. 5 and Fig. 6. It can be noted that for two joint velocities $(\dot{q}_1, \dot{q}_6)$, it is decaying during the whole operation time. However, for the translation velocity (q_4) of tube 1, the curve is different which can be explained by high level of non-linearity of the robot forward kinematics. Nevertheless, the desired position is achieved with an error inferior to 10^{-5} m^2 in 40 iterations.

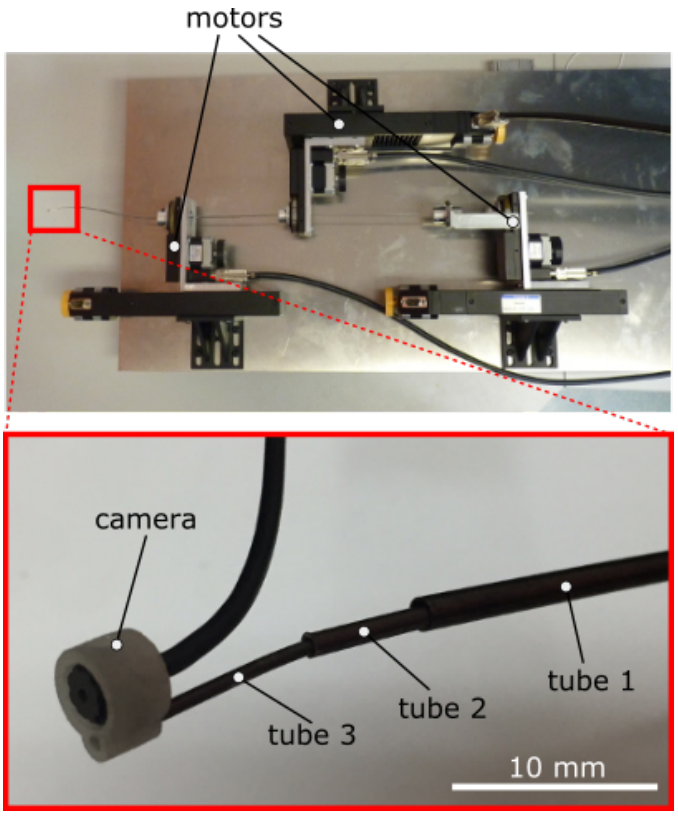

Fig. 4. Experimental setup of the validation of the proposed control scheme. *Top*: general view on the setup; each motor controls two degrees of freedom, one rotation and one translation. *Bottom*: zoom on the robot's end-effector with camera mounted on the tube 3.

Contrary to the simulation validation in which 6 DOF positioning tasks were successfully achieved, the experimental validation is limited to 3 DOF. This is due to the fact that certain motors which compose our prototype cannot be controlled in velocity and are not equipped with coders.

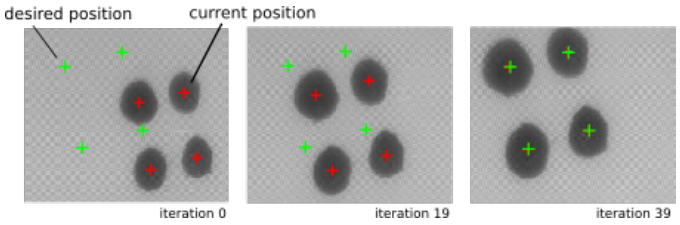

Fig. 5. Robot performing positioning task using IBVS. Images correspond to the experiment presented in Section IV-B1.

2) Adaptive gain for fast convergence: As mentioned previously, the kinematic model of the robot is highly non-linear. It results in the fact that the impact of each joint variable on the final position of the robot's end-effector is very different. Thus, in order to compensate this effect and to ensure better and faster convergence, the IBVS scheme with adaptive gain is proposed. It means that the value of the gain λ in equation (4) should be different for every joint. Therefore, it transform to a vector $\boldsymbol{\lambda} = (\lambda_1, ..., \lambda_n)^\top$, containing six entries in our case, with λ_i corresponding to joint variable q_i. The values

Listing 1. Pseudo-code for visual servoing of CTR

```
//include ViSP files
#include <vpRobotRTC.h>

int main(){
  // Initialization
  vpRobotRTC robot;
  vpServo task;
  task.setServo(vpServo::EYEINHAND_L_cVe_eJe);
  vpDot2 dots[4];
  task.addFeatures(dots);

  bool task_finished = false;
  while (!task_finished) // visual servo loop
  {
    vpImage I = getImage();
    dots.track(I);
    vpColVector v = task.computeControlLaw();
    robot.setVelocity(vpRobot::ARTICULAR_FRAME, v);
    double error = task.getError().sumSquare();

    if (error < 1e-5) task_finished = true;
  }
}
```

of λ_i were determined experimentally. Moreover, we also suggest adding an adjustment function in order to change the gains depending on the value of the error. It means that the gain should be increased if the pixel error in the image decreases. Thus, the final expression for gain computation at every iteration is written as

$$\lambda_i' = \lambda_i + c_1 \exp(-c_2 e^2); \tag{17}$$

where λ_i' is the adaptive gain; c_1 and c_2 are two constants defining the properties of gain adjustment; e is the mean distance in pixels between points in desired and current positions. The constant c_1 defines the maximal value that can be added to the initial gain, thus, its maximal amplitude. The constant c_2 determines the starting point of adjustment, in other words, the value of error from which the adaptation takes effect. For example, for c_2 = 0.01, the adjustment starts from the error inferior to 25 pixels. In present work, we used c_1 = 80 and c_2 = 0.01. Both values were determined experimentally.

The results of positioning task realization are shown in Fig. 7. In contrast to the previous experiment with constant gain, the desired position is now achieved in 14 iterations, thus, three times faster. Moreover, for all joints, the velocity tends to be exponentially decaying.

3) Moving desired position: The last experiment presented here consisted in testing the control scheme in case of moving desired position. Mainly, it corresponds to performing several consecutive positioning tasks while updating the desired position (Fig. 8). As can be noticed, the positioning error is maintained to zero despite the motion of the desired position. For instance, this can useful for virtual compensation (in the image) of physiological movements during surgical interventions.

V. Conclusion

In this paper, a model for CTR with three tubes is proposed allowing to establish a direct link between curvature

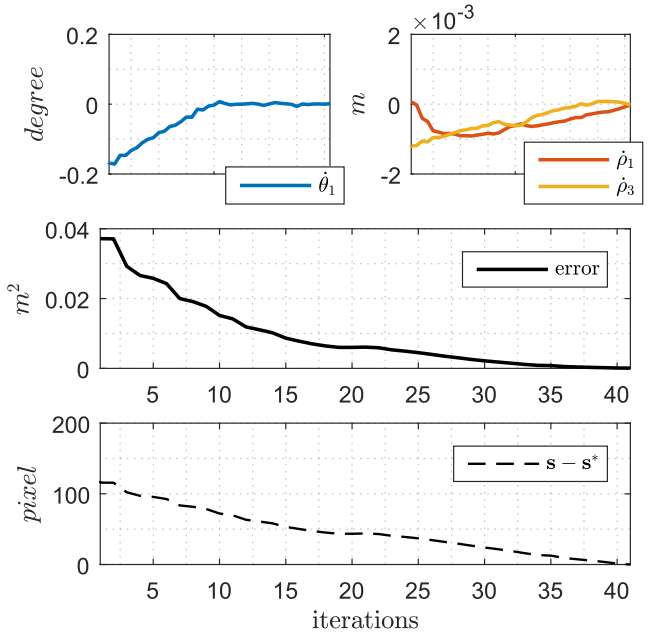

Fig. 6. 3D positioning of CTR. *Top:* joint velocities, *bottom:* evolution of error.

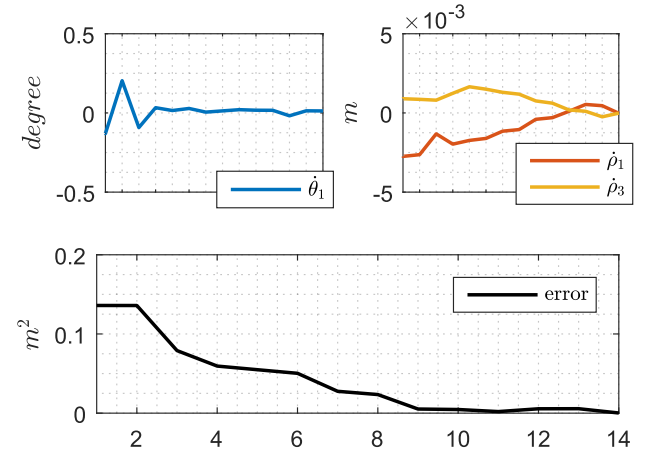

Fig. 7. 3D positioning of CTR with adaptive gain. *Top:* joint velocities, *bottom:* evolution of error.

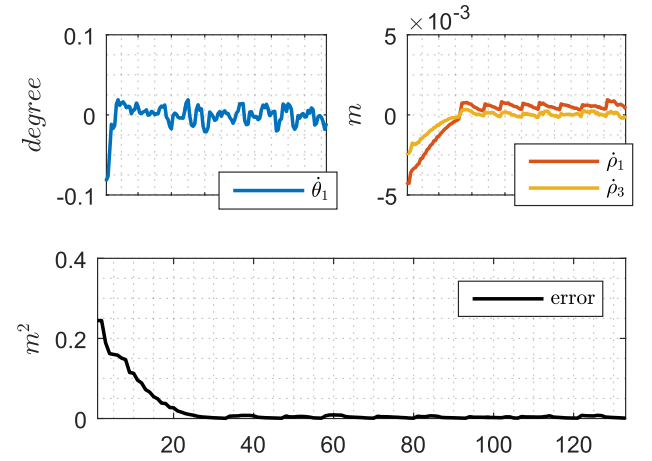

Fig. 8. CTR control using visual servoing with adaptive gain and moving desired position. *Top:* joint velocities, *bottom:* evolution of error.

parameters of the tubes and the actuation drives. Both forward kinematics and final robot Jacobian are presented. It allowed then to develop a new control scheme for such type of robots based on IBVS techniques. Thanks to the camera mounted on the tip of the robot, thus serving as the robot's end-effector, it is now possible to control the robot with high level of accuracy. In fact, the eye-in-hand configuration presents several advantages comparing to classical setup with a static camera looking at the robot tool (eye-to-hand configuration). First, the robot is now capable to operate in a confined space as the camera moves with the robot. Secondly, it allows avoiding the problem of limited depth-of-field.

Further, the robot is controlled in a closed loop using visual servoing approaches. The presented scheme has been validated first in simulation and then on a real experimental setup. The results are very promising as the final positioning error is below 10^{-5} m^2, or, in other words, less than one pixel. Moreover, the implementation of adaptive gain allows not only reaching the desired position in fewer iterations but only to partly compensate the non-linearity of the robot model.

Finally, for the ease of future use, all presented algorithms were implemented within ViSP library. Thanks to two new developed classes it is possible to investigate the robot performances (repeatability, robustness and stability) regardless of the recurrent technical issues of lab-made experimental setup.

VI. Future work

Future work will concern mostly the experimental part of the project. First, it is important to extend the experimental validation to 6 DOF one we replace the robotic platform motors (especially the rotations ones) which do not allow velocity-based control at the current state

Secondly, in present work, we used a target containing four black blobs for tracking. As this robot is dedicated mainly for medical applications the target object may also be replaced by a target more similar to biological sample. Moreover, later the white camera will be replaced by OCT probe (which will be co-axial with robot tubes). The ultimate idea is to be able to perform *in-situ* investigation by controlling the collection of optical biopsies of suspected tissue or organ.

Acknowledgment

This work has been supported by the Labex ACTION project (contract "ANR-11-LABX-0001-01") and ANR NEMRO (contract "ANR-14-CE17-0013").

References

[1] J. Burgner-Kahrs, D. C. Rucker, and H. Choset, "Continuum robots for medical applications: A survey," *IEEE Trans. on Robotics*, vol. 31, no. 6, pp. 1261–1280, 2015.

[2] H. B. Gilbert, D. C. Rucker, and R. J. Webster III, "Concentric tube robots: The state of the art and future directions," in *Int. Symp. Rob. Res.*, 2013.

[3] D. B. Camarillo, C. F. Milne, C. R. Carlson, M. R. Zinn, and J. K. Salisbury, "Mechanics modeling of tendon-driven continuum manipulators," *IEEE Trans. on Robotics*, vol. 24, no. 6, pp. 1262–1273, 2008.

[4] M. Cianchetti, T. Ranzani, G. Gerboni, I. De Falco, C. Laschi, and A. Menciassi, "Stiff-flop surgical manipulator: mechanical design and experimental characterization of the single module," in *IEEE/RSJ Int. Conf. on Intelligent Robots and Systems*, 2013, pp. 3576–3581.

[5] M. Farajollahi, V. Woehling, C. Plesse, G. T. Nguyen, F. Vidal, F. Sassani, V. X. Yang, and J. D. Madden, "Self-contained tubular bending actuator driven by conducting polymers," *Sensors and Actuators A: Physical*, vol. 249, pp. 45–56, 2016.

[6] H. Su, G. Li, D. C. Rucker, R. J. Webster III, and G. S. Fischer, "A concentric tube continuum robot with piezoelectric actuation for MRI-guided closed-loop targeting," *Annals of Biomedical Engineering*, pp. 1–11, 2016.

[7] I. S. Godage, A. A. Remirez, R. Wirz, K. D. Weaver, J. Burgner-Kahrs, and R. J. Webster, "Robotic intracerebral hemorrhage evacuation: An in-scanner approach with concentric tube robots," in *IEEE/RSJ Int. Conf. on Intelligent Robots and Systems*, 2015, pp. 1447–1452.

[8] C. Nadeau, H. Ren, A. Krupa, and P. Dupont, "Intensity-based visual servoing for instrument and tissue tracking in 3D ultrasound volumes," *IEEE Trans. on Automation Science and Engineering*, vol. 12, no. 1, pp. 367–371, 2015.

[9] Y. Baran, K. Rabenorosoa, G. J. Laurent, P. Rougeot, N. Andreff, and B. Tamadazte, "Preliminary results on oct-based position control of a concentric tube robot," in *IEEE/RSJ Int. Conf. on Intelligent Robots and Systems*, 2017.

[10] M. Ourak, B. Tamadazte, and N. Andreff, "Partitioned camera-oct based 6 DOF visual servoing for automatic repetitive optical biopsies," in *IEEE/RSJ Int. Conf. on Intelligent Robots and Systems*, 2016, pp. 2337–2342.

[11] J.-A. Seon, B. Tamadazte, and N. Andreff, "Decoupling path following and velocity profile in vision-guided laser steering," *IEEE Trans. on Robotics*, vol. 31, no. 2, pp. 280–289, 2015.

[12] G. Chesi, K. Hashimoto, D. Prattichizzo, and A. Vicino, "Keeping features in the field of view in eye-in-hand visual servoing: a switching approach," *IEEE Trans. on Robotics*, vol. 20, no. 5, pp. 908–914, 2004.

[13] J. Burgner, D. C. Rucker, H. B. Gilbert, P. J. Swaney, P. T. Russell, K. D. Weaver, and R. J. Webster, "A telerobotic system for transnasal surgery," *IEEE/ASME Trans. on Mechatronics*, vol. 19, no. 3, pp. 996–1006, 2014.

[14] H. Yu, L. Wu, K. Wu, and H. Ren, "Development of a multi-channel concentric tube robotic system with active vision for transnasal nasopharyngeal carcinoma procedures," *IEEE Robotics and Automation Letters*, vol. 1, no. 2, pp. 1172–1178, 2016.

[15] J. A. Piepmeier and H. Lipkin, "Uncalibrated eye-in-hand visual servoing," *The Int. J. of Robotics Research*, vol. 22, no. 10-11, pp. 805–819, 2003.

[16] K. Wu, L. Wu, C. M. Lim, and H. Ren, "Model-free image guidance for intelligent tubular robots with pre-clinical feasibility study: towards minimally invasive trans-orifice surgery," in *IEEE Int. Conf. on Information and Automation*, 2015, pp. 749–754.

[17] B. Espiau, F. Chaumette, and P. Rives, "A new approach to visual servoing in robotics," *IEEE Trans. on Robotics and Automation*, vol. 8, no. 3, pp. 313–326, 1992.

[18] G. Flandin, F. Chaumette, and E. Marchand, "Eye-in-hand/eye-to-hand cooperation for visual servoing," in *IEEE Int. Conf. on Robotics and Automation*, vol. 3, 2000, pp. 2741–2746.

[19] É. Marchand, F. Spindler, and F. Chaumette, "VISP for visual servoing: a generic software platform with a wide class of robot control skills," *IEEE Robotics & Automation Magazine*, vol. 12, no. 4, pp. 40–52, 2005.

[20] T. T. H. Tran and E. Marchand, "Real-time keypoints matching: application to visual servoing," in *IEEE Int. Conf. on Robotics and Automation*, 2007, pp. 3787–3792.

[21] N. Andreff, B. Espiau, and R. Horaud, "Visual servoing from lines," *Int. J. of Robotics Research*, vol. 21, no. 8, pp. 679–700, 2002.

[22] C. Collewet and E. Marchand, "Photometric visual servoing," *IEEE Trans. on Robotics*, vol. 27, no. 4, pp. 828–834, 2011.

[23] B. Tamadazte, N. Piat and E. Marchand, "A Direct Visual Servoing Scheme for Automatic Nanopositioning, " *IEEE/ASME Trans. on Mechatronics*, vol. 17, no. 4, pp. 728-736, 2012.

[24] L.-A. Duflot, A. Krupa, B. Tamadazte, and N. Andreff, "Shearlet-based vs. photometric-based visual servoing for robot-assisted medical applications," in *IEEE/RSJ Int. Conf. on Intelligent Robots and Systems*, 2016, pp. 4099–4104.

[25] M. Ourak, B. Tamadazte, O. Lehmann, and N. Andreff, "Wavelets-based 6 DOF visual servoing," in *IEEE Int. Conf. on Robotics and Automation*, 2016, pp. 3414–3419.

[26] R. J. Webster III and B. A. Jones, "Design and kinematic modeling of constant curvature continuum robots: A review," *The Int. J. of Robotics Research*, vol. 29, pp. 1661–1683, 2010.

[27] B. A. Jones and I. D. Walker, "A new approach to jacobian formulation for a class of multi-section continuum robots," in *Int. Conf. on Robotics and Automation*, 2005, pp. 3268–3273.

[28] R. M. Murray, Z. L. Li, and S. S. Sastry, *A Mathematical Introduction to Robotic Manipulation*, R. M. Murray, Z. L. Li, and S. S. Sastry, Eds, CRC Press, 1994.

[29] R. J. Webster, A. M. Okamura, and N. J. Cowan, "Toward active cannulas: Miniature snake-like surgical robots," in *IEEE/RSJ Int. Conf. on Intelligent Robots and Systems*, 2006, pp. 2857–2863.

[30] P. Sears and P. Dupont, "A steerable needle technology using curved concentric tubes," in *IEEE/RSJ Int. Conf. on Intelligent Robots and Systems*, 2006, pp. 2850–2856.

[31] R. Hartley and A. Zisserman, *Multiple view geometry in computer vision*, Cambridge university press, 2003.